Clim Dyn (2011) 36:491–507
DOI 10.1007/s00382-010-0910-3

Simulation of regional climate change under the IPCC A2 scenario in southeast China

Weilin Chen · Zhihong Jiang · Laurent Li · Pascal Yiou

Received: 4 June 2009 / Accepted: 10 September 2010 / Published online: 29 September 2010

Abstract A variable-grid atmospheric general circulation model, LMDZ, with a local zoom over southeast China is used to investigate regional climate changes in terms of both means and extremes. Two time slices of 30 years are chosen to represent, respectively, the end of the 20th century and the middle of the 21st century. The lower-boundary conditions (sea-surface temperature and sea-ice extension) are taken from the outputs of three global coupled climate models: Institut Pierre-Simon Laplace (IPSL), Centre National de Recherches Météorologiques (CNRM) and Geophysical Fluid Dynamics Laboratory (GFDL). Results from a two-way nesting system between LMDZ-global and LMDZ-regional are also presented. The evaluation of simulated temperature and precipitation for the current climate shows that LMDZ reproduces generally well the spatial distribution of mean climate and extreme climate events in southeast China, but the model has systematic cold biases in temperature and tends to overestimate the extreme precipitation. The two-way nesting model can reduce the "cold bias" to some extent compared to the one-way nesting model. Results with greenhouse gas forcing from the SRES-A2 emission scenario show that there is a significant increase for mean, daily-maximum and minimum temperature in the entire region, associated with a decrease in the number of frost days and an increase in the heat wave duration. The annual frost days are projected to significantly decrease by 12–19 days while the heat wave duration to increase by about 7 days. A warming environment gives rise to changes in extreme precipitation events. Except two simulations (LMDZ/GFDL and LMDZ/IPSL2) that project a decrease in maximum 5-day precipitation (R5d) for winter, other precipitation extremes are projected to increase over most of southeast China in all seasons, and among the three global scenarios. The domain-averaged values for annual simple daily intensity index (SDII), R5d and fraction of total rainfall from extreme events (R95t) are projected to increase by 6–7, 10–13 and 11–14%, respectively, relative to their present-day values. However, it is clear that more research will be needed to assess the uncertainties on the projection in future of climate extremes at local scale.

Keywords Climate change · Climate extremes · Variable-grid model · Southeast China

W. Chen · Z. Jiang (✉)
Key Laboratory of Meteorological Disaster of Ministry of Education, Nanjing University of Information Science and Technology, Nanjing, China
e-mail: zhjiang@nuist.edu.cn

W. Chen
e-mail: wl_chenchen@163.com

L. Li
Laboratoire de Météorologie Dynamique, IPSL/CNRS/UPMC, Paris, France

P. Yiou
Laboratoire des Sciences du Climat et de l'Environnement, IPSL, UMR CNRS-CEA-UVSQ, CE Saclay l'Orme des Merisiers, Gif-sur-Yvette, France

1 Introduction

Atmosphere–Ocean General Circulation Models (AOGCMs) are important tools for projecting the climate under scenarios of greenhouse gas emission. However, due to their coarse spatial resolution (typically, the horizontal resolution of AOGCMs participating in IPCC AR4 ranges from 400 to 125 km, Meehl et al. 2007), they cannot provide information at scales finer than their computational grid.

But processes at the unresolved scales are important. This is particularly the case in East Asia, where AOGCMs always have large biases in reproducing the present-day climate, due to the complex topography (Zhou and Li 2002; Gao et al. 2004, 2006; Jiang et al. 2005; Zhou and Yu 2006) that affect the East Asian Monsoon. Furthermore, the skill of AOGCMs in simulating climate extremes in this region is also poor (Jiang et al. 2009; Wang et al. 2008). As a result, outputs of the AOGCMs can hardly be directly used in impact-oriented studies, and downscaling is necessary to obtain data at appropriate scales.

Two downscaling techniques, dynamical and empirical statistical, have been developed to bridge the gap between the coarse resolution of climate models output and the need for surface weather variables at finer spatial resolution. "Statistical downscaling" models statistical relationships between the local climates (predictand) and carefully selected large-scale parameters (predictor) (Wilby et al. 2004; Wetterhall et al. 2006; Goodess et al. 2007). "Dynamical downscaling", on the other hand, uses a high-resolution limited-area model nested into the global models (Frei et al. 2006). This approach allows taking into account the detailed regional topography to ensure a better simulation of local weather events and climate. The above-mentioned two methods can also be used simultaneously in order to examine uncertainties of downscaling (Haylock et al. 2006; Schmidli et al. 2007). Another existing approach used to generate regional climate information is based on the use of variable-resolution (zoomed) atmosphere general circulation models with higher resolution for the region of interest (Gibelin and Déqué 2003; Goubanova and Li 2007). Results from variable-resolution GCMs capture, over the high-resolution region, finer-scale details than uniform-resolution models while retaining global skill similar to uniform-resolution simulations with the same number of grid points.

For China, a number of recent climate change simulations with different regional climate models have been analyzed for future variation in both mean climate and climate extremes. For example, Zhang et al. (2006) studied the distribution of the present and future extreme climate events in China under the IPCC SRES B2 scenario with the PRECIS (Providing REgional Climates for Impacts Studies, Jones et al. 2004) climate model. They indicate that, in the future, the occurrence of hot events is projected to be more frequent while the occurrence of cold events is likely to be much rarer. There would be an overall increasing trend in extreme precipitation over most of China especially in the southeast coastal zone and in the middle and lower reaches of the Yangtze River. Gao et al. (2008) studied climate changes over East Asia using RegCM3, nested within the NASA/NCAR global model FvGCM. Tang et al. (2008) investigated regional climate changes in China under the IPCC A2 scenario by using MM5V3 nested in the CISRO Mark 3 global climate model. They found that surface air temperature in China would increase in the future, with a stronger trend in winter and a south-north increasing gradient. Gao et al. (2006) reported that simulated East Asia large-scale precipitation patterns are significantly affected by model resolution. Furthermore, they found that model resolutions of 60 km or finer are needed to accurately simulate the distribution of precipitation over China. However, the above-mentioned models (e.g., PRECIS, RegCM3 and MM5V3) are all nested regional climate models, and variable-resolution GCMs have rarely been used in climate change simulations over China.

In the present study, we estimate future changes of daily temperature and precipitation statistics in southeast China by using a variable-resolution GCM with a stretched grid. The main objective of our study is to document simulated changes of extremes in southeast China for both temperature and precipitation. Climate extremes are expressed in terms of extreme indices (Frich et al. 2002; STARDEX 2005; Alexander et al. 2006; Tebaldi et al. 2006). We address the issue of uncertainties by taking into account SST (sea-surface temperature) and sea ice variations from three different global coupled GCMs.

The paper is organized as follows. Section 2 describes the model, data and methodologies used in this study. Results of the model evaluation in southeast China are discussed in Sect. 3. The scenarios of climate change are presented and interpreted in Sect. 4. Finally, Sect. 5 summarizes the results and draws conclusions.

2 Study region, model, simulations and diagnostics

2.1 Study region, model and simulations

The study area encompasses the region of southeast China. The most distinctive climatic feature of this region is the East Asian monsoon. Precipitation is affected by both the strength of the monsoonal flows and the amount of water vapour transported. Summer precipitation accounts for 60–85% of the annual total precipitation. It yields a decreasing gradient from south-east to north-west. In winter, surface air temperature sharply drops from south to north as a function of the intensity of the East Asian winter monsoon, which carries cold air from the polar region into East Asia. The topographic structure of the region is displayed in Fig. 1a. The area is generally characterized by an increasing elevation from southeast to northwest. The complex regional topography has strong influences on the local climate and its spatial variability (Gao et al. 2006; Wu et al. 2007; Liu et al. 2007).

LMDZ is the atmospheric general circulation model developed in the Laboratoire de Météorologie Dynamique

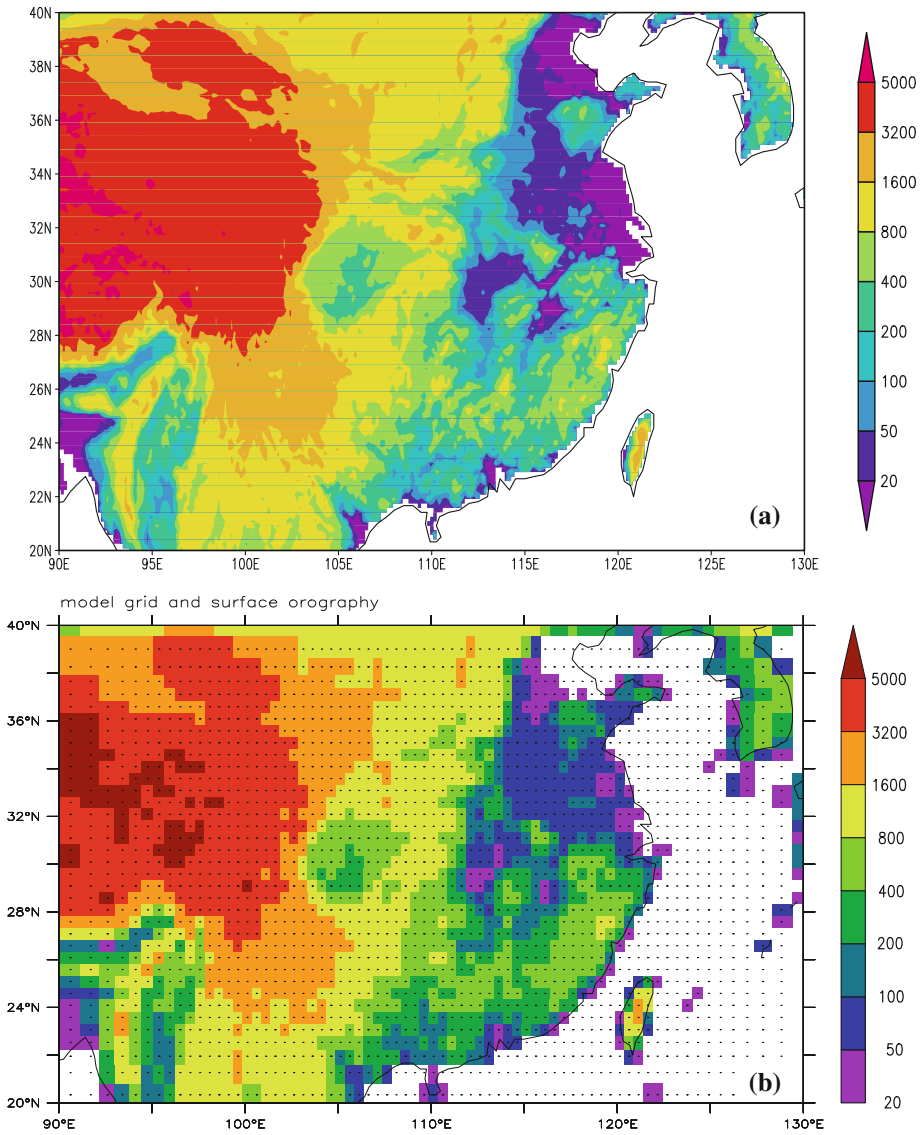

Fig. 1 **a** Real orography (GTOPO30, Global 30 Arc Second Elevation Data Set, http://eros.usgs.gov/#/Find_Data/Products_and_Data_Available/gtopo30_info) and **b** grid and surface orography (*bottom*, color shading in m) of LMDZ-regional, *black markers* indicate LMDZ-regional grid cell centers

in Paris. It is a grid-point model with a state-of-the-art physical parameterization (Li 1999, Hourdin et al. 2006). LMDZ is also the atmospheric component of the coupled climate system model used in IPSL (Institut Pierre-Simon Laplace) for the climate change scenarios reported in IPCC-AR4 (Solomon 2007). Two versions of LMDZ are used in this study: LMDZ-global and LMDZ-regional. They share an identical physical parameterization, and differ only by their horizontal resolutions. LMDZ-global has a globally uniform resolution of 2.5° in latitude and 3.75° in longitude. LMDZ-regional uses the zoom ability to increase the spatial resolution over the Yangtze River basin. The zoom is centred at 30°N/110°E and covers roughly a domain of 40° in longitude and 20° in latitude. For this domain, the model has the spatial resolution from 0.50° to 0.55° in latitude and longitude. Figure 1b shows the model grid and surface orography of LMDZ-regional. For southeast China, we can roughly follow the three-step orography from southeast to northwest. The first step is the coastal region with large plains in the north and small mountains (less than 400 m of altitude) in the south. The second step comprises regions with altitude from 400 to 1,600 m. The third step is the Tibetan Plateau with altitude passing over 5,000 m. The Sichuan basin centered at 105°E/30°N is very well depicted by LMDZ-regional. Note that the Yangtze River crosses the Sichuan basin and goes eastward following roughly the latitude 30°N.

Although LMDZ-regional is a global model with local zoom, it is indeed used as a traditional limited-area model with the whole globe (except the zoomed domain) as buffer zone that receives outputs of LMDZ-global. An exponential relaxation procedure for atmospheric temperature and circulation (u and v for wind) is applied in the buffer zone with a time scale of 30 min. The same version of

Table 1 List of simulations conducted with LMDZ for different periods and with different boundary conditions

Simulation	Period	Boundary conditions
LMDZ/CTRL	Present-day	Climatological SST and sea-ice, one-way nesting
LMDZ/IPSL	About 2045	SST and sea-ice from IPSL global model IPCC-A2 scenario
LMDZ/CNRM	About 2045	SST and sea-ice from CNRM global model IPCC-A2 scenario
LMDZ/GFDL	About 2045	SST and sea-ice from GFDL global IPCC-A2 scenario
LMDZ/CTRL2	Present-day	Same as LMDZ/CTRL, but two-way nesting
LMDZ/IPSL2	About 2045	Same as LMDZ/IPSL, but two-way nesting

LMDZ-regional for southeast China was already used in Zou et al. (2010), but relaxed to ERA-40 data from 1958 to 2001. Zou et al. (2010) concluded that such a dynamical downscaling improves not only the climatology of monsoon major rain band but also the inter-annual variability modes of rainfall over eastern China in comparison to that of ERA40. The added values of LMDZ-regional were evident in both the spatial patterns of dominant rainfall variability modes and the associated temporal variations.

The main simulations presented in this paper are performed through the combination of LMDZ-global and LMDZ-regional working in tandem and in a sequential manner: atmospheric temperature and winds from LMDZ-global enter into LMDZ-regional every 6 h but there is no feedback from LMDZ-regional to LMDZ-global. Furthermore, we also present results from a two-way nesting system between LMDZ-global and LMDZ-regional. Through two-way nesting, the two models run in parallel with information exchanged every 2 h: outputs of LMDZ-global (LMDZ-regional) as boundary conditions for LMDZ-regional (LMDZ-global) outside (inside) the domain of interest. The two-way nesting is an optimal treatment for interactions between regional and global scales. Lorenz and Jacob (2005) showed already that the two-way nesting can improve the global climate through a better representation of a region (the Maritime Continent area, in their study).

The control simulations representing present-day climate are performed through the tandem of LMDZ-global and LMDZ-regional with seasonally-varying climatological SST and sea-ice averaged from 1961 to 1990 and concentration of different greenhouse gases for the same period. For future climate, we choose the SRES-A2 emission scenario for our targeted period around 2045. We use the monthly-mean SST and sea ice (averaged from 2041 to 2050) obtained from global coupled climate system models as a surrogate to assess the climate change at regional scales. As demonstrated in Gastineau et al. (2009), main signals of the atmospheric circulation under global warming can be retrieved from the global SST. Furthermore, we adopt the approach of differential SST, which consists of adding the predicted SST variation (monthly-mean seasonal cycle of 2041/2050 minus 1961/1990) from global models to the observed monthly-mean and seasonally-varying climatological SST (period 1961/1990). This differential approach was also used in Goubanova and Li (2007) for climate downscaling in the Mediterranean region. It gives the best results for the present-day control simulation, which uses the observed lower-boundary conditions. It is also useful to compare downscaled results from different global models, since they share a same control climate. Sea ice is also treated in a differential manner, in proportion to the variation of ice-covered surface in global models for each hemisphere. To increase our confidence, we use the SST and sea-ice outputs from three different global climate system models, developed and run in IPSL (Dufresne et al. 2002), CNRM (Gibelin and Déqué 2003) and GFDL (Delworth et al. 2002), respectively. The corresponding simulations with LMDZ will be referred to as LMDZ/IPSL, LMDZ/CNRM and LMDZ/GFDL, and the two-way nesting system from LMDZ-global and LMDZ-regional is referred to as LMDZ/IPSL2. In addition, control simulations of the one-way nesting system and the two-way nesting one are referred to as LMDZ/CTRL and LMDZ/CTRL2, respectively, as shown in Table 1. Note that future-climate scenarios are run also with the corresponding future concentration of greenhouse gases. All simulations are performed for 30 years with climatological SST and sea ice. Our experimental design with climatological lower-boundary conditions eliminates variability from inter-annual to inter-decadal time scales and allows obtaining a stationary sampling that simplifies diagnostics on climate extremes. Finally, we point out that our choice of a 10-year period 2041/2050 for future climate may be a little short to eliminate inter-annual variability of global coupled models. But it is a result of the consideration that we would avoid using a longer interval and consequently averaging too-much different climate parameters. In fact, the middle of the 21st century is a quick transition period in our simulations.

2.2 Daily temperature and precipitation statistics

For the validation of the control simulations, we use two observational datasets for temperature and precipitation, respectively. The observed daily mean, daily maximum and minimum temperatures were obtained from a new daily

temperature dataset on a 0.5° × 0.5° grid developed by Xu et al. (2009). The dataset is deduced from 751 meteorological stations over mainland China. A topographic correction was applied during the grid interpolation.

As for the daily total precipitation amounts, we use a daily gridded dataset provided by Chen et al. (2010), with a resolution of 0.5° by 0.5°, comparable to LMDZ. This dataset is also deduced from 753 operational surface stations of the China Meteorological Administration by an ordinary kriging interpolation, with small interpolation errors in the eastern part of China owing to the high station density. We also used another gridded precipitation dataset offered by Xie et al. (2007) to evaluate the simulation. Similar evaluation results are found between Chen and Xie's datasets so that the latter are not shown.

In this study we use nine daily temperature and precipitation statistics as shown in Table 2. There are five temperature-related diagnostics. Tav, Tx and Tn are the mean values in a season or a year for average temperature, daily maximum temperature and minimum temperature, respectively. The frost days (FD) are an indicator measuring the number of frost days for a given season or year. The heat wave duration index (HW) is defined as the number of consecutive days in a given season for which the daily maximum temperature on each day exceeds the long-term 90% quantile of the corresponding calendar day's maximum temperature, which is calculated as average of the daily maximum temperature over a 5-day window centred on that calendar day (Hundecha and Bardossy 2008). It is a useful indicator for measuring prolonged periods of heat stress in summer or in a year calculated from daily maximum temperatures. Besides the mean precipitation (Pav), there are three precipitation extreme indices (SDII, R5d, R95t). SDII is a measure of the average amount of precipitation that falls on a wet day in a given season or a year, while R95T and R5d measure the magnitude of the most intense precipitation events. The indices were calculated using the STARDEX project (Goodess 2003) diagnostic tool as described in the web site of the project.

3 Evaluation of the LMDZ-regional ability to simulate observed climate in southeast China

3.1 Spatial patterns

Figure 2 compares the spatial distribution of the annual-mean temperature, daily-maximum temperature, and daily-minimum temperature of the two control simulations (LMDZ/CTRL and LMDZ/CTRL2) with observations. The two simulations reproduce well the general patterns of temperature decrease from south to north, as well as the sub-peak over the Sichuan basin (28°–32°N, 104°–108°E). The spatial pattern correlation coefficients between simulated and observed annual-mean Tav, Tx and Tm are 0.97, 0.95 and 0.97, respectively, for LMDZ/CTRL, and 0.96, 0.93, and 0.96, respectively, for LMDZ/CTRL2. However, the simulated temperatures of LMDZ/CTRL tend to be lower than the observed ones, especially in the northern parts of this region, where biases are up to −5°C. The two-way nesting LMDZ/CTRL2 reduces such systematic cold biases remarkably. In particular, LMDZ/CTRL2 shows a warm bias of up to 1–2°C in eastern parts. Careful examination reveals that this amelioration is a direct consequence of changes in the large-scale atmospheric circulation, due to the feedbacks from the regional model to the global one. Figure 3 shows the differences of annual-mean 700-hPa geopotential height (contour) and atmospheric circulation (wind vectors) between observations (from the 40-year European Centre for Medium-Range Weather Forecasts (ECMWF) Re-Analysis (ERA-40), Uppala 2005) and the

Table 2 Diagnostics of daily temperature and precipitation used in this study

Indices	Definition	Units
Tav	Mean temperature averaged in a season or a year	°C
Tx	Mean daily-maximum-temperature averaged in a season or a year	°C
Tn	Mean daily-minimum-temperature averaged in a season or a year	°C
FD	Total number of frost days (daily-minimum-temperature <0°C)	days
HW[a]	Percentile-based heat have duration	days
Pav	Mean precipitation averaged in a season or a year	mm/day
SDII	Simple daily intensity index: mean precipitation on days with precipitation ≥ 1 mm	mm/day
R5d	Maximum total precipitation from any consecutive 5 days	mm
R95t	Heavy rainfall proportion: fraction of total rainfall from events >95th percentile	%

[a] This index is defined as the number of consecutive days in a given season for which the daily maximum temperature on each day exceeds the long-term 90% quantile of the corresponding calendar day's maximum temperature, which is calculated as average of the daily maximum temperature over a 5-day window centred on that calendar day

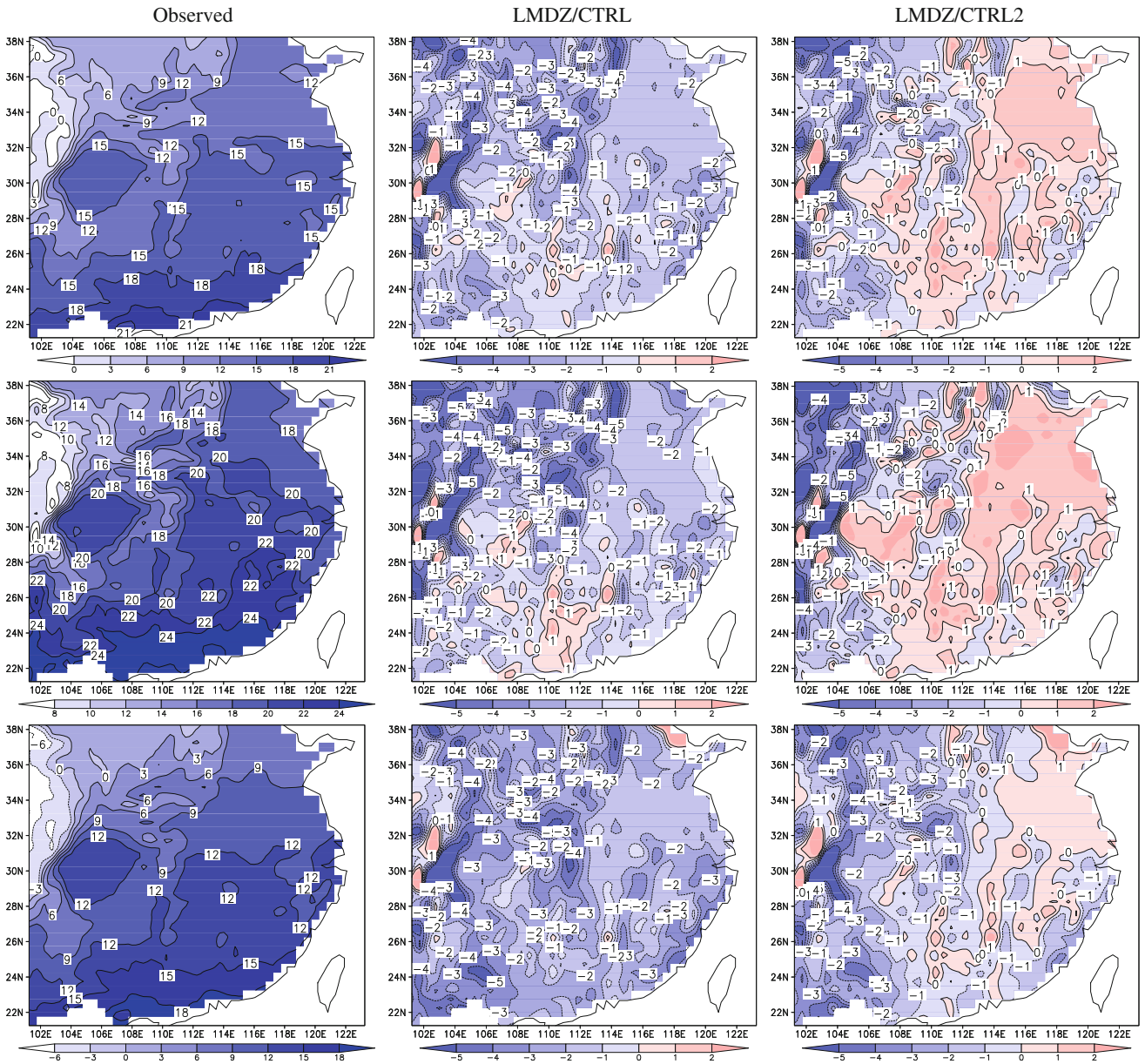

Fig. 2 Observed spatial distributions of present-day climate parameters (*left three panels*), differences between observations and LMDZ/CTRL (*middle three panels*) and LMDZ/CTRL2 (*right three panels*). Annual-mean Tav are on the *top* three panels, Tx on the *middle three panels*, and Tn on the *bottom panels*. The parameters Tav, Tx and Tn are introduced in Table 2. Units are °C

two control simulations LMDZ/CTRL (top plot) and LMDZ/CTRL2 (bottom plot). It is clear that the inclusion of a detailed representation in southeast China modifies strongly the atmospheric circulation around this region. For LMDZ/CTRL (top plot), We found that compared to observation, a large anomalous cyclone takes place over Japan and Northeastern Asia, which intensifies the northwesterly wind anomaly toward southeast China, thus, conveying more cold air from north. This may explain the existence of the above-mentioned large "cold bias" of LMDZ/CTRL. However, for LMDZ/CTRL2, the cyclonic anomaly over Japan is much weaker than that of LMDZ/CTRL. Correspondingly, the anomalous northwesterlies over southeast China are weakened (bottom plot) As a result, the cold biases of LMDZ/CTRL2 are reduced.

Figure 4 shows observed spatial distribution, as well as the fractional differences between observed and simulated fields of the annual-mean precipitation, annual SDII, and R5d, respectively, for present-day climate in southeast China. The observed Pav, SDII, and R5d decrease from southeast to northwest. Overall, the model results reproduce the broad spatial patterns of observed precipitation-related indices, the spatial pattern correlation coefficients

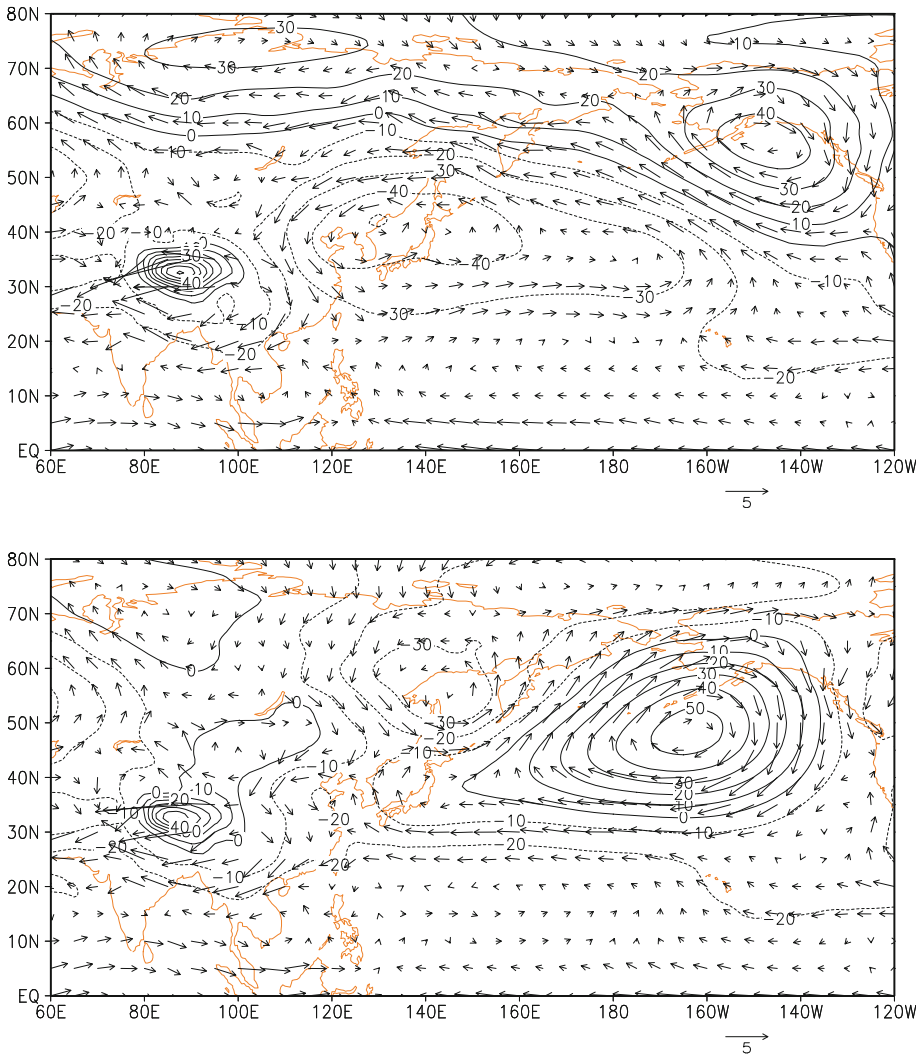

Fig. 3 Differences of 700-hPa geopotential height (contour, m) and wind vectors between observations the two control simulations LMDZ/CTRL (*top plot*) and LMDZ/CTRL2 (*bottom plot*). The latter has the regional model (LMDZ-regional) over southeast China running interactively (two-way nesting between LMDZ-global and LMDZ-regional)

between models results and observed Pav, SDII, and R5d are 0.8, 0.7 and 0.6, respectively, for LMDZ/CTRL2, and 0.7, 0.6, 0.5, respectively, for LMDZ/CTRL. However, both models tend to underestimate Pav, SDII and R5d in the southern parts of this area, with a magnitude varying from −10 to −40%. Conversely, in the northwestern parts the Pav and R5d are overestimated severely by both LMDZ/CTRL and LMDZ/CTRL2. For SDII, simulated values are obviously lower in entire southeast China except in the northwestern regions as already mentioned. It is also worth noting that although LMDZ/CTRL and LMDZ/CTRL2 share similar spatial pattern in general, there exist large differences in the simulation of precipitation amounts between them. Overall, LMDZ/CTRL has much more precipitation than in LMDZ/CTRL2. The domain-averaged biases of annual-mean Pav, SDII and R5d are +16.9, −4.0% and +35.5%. respectively, for LMDZ/CTRL, and −0.7, −17.5 and 6.8%, respectively, for LMDZ/CTRL2. These differences are mainly due to a drastic reduction of extreme/intense precipitation in LMDZ/CTRL2 compared to LMDZ/CTRL (as shown later in Fig. 6).

For other indices and seasons, we calculated the spatial correlation coefficient between the observed and simulated fields for both LMDZ/CTRL and LMDZ/CTRL2 as shown in Fig. 5. Spatial correlation coefficient for T, Tmax and Tmin is high with values larger than 0.9 in all seasons for both LMDZ/CTRL and LMDZ/CTRL2, suggesting that the two models can simulate well the distribution of most temperature-related diagnostics, with the exception of the percentile-based HW. The performance of the model in constructing precipitation-related diagnostics is less satisfactory than its performance for temperature-related diagnostics. Furthermore, LMDZ/CTRL and LMDZ/CTRL2 simulate well both mean and extreme precipitation field in winter, while its performance in summer is deteriorated. Compared to LMDZ/CTRL, the improvement of LMDZ/CTRL2 is seen in the spatial correlation coefficient for HW and Pav.

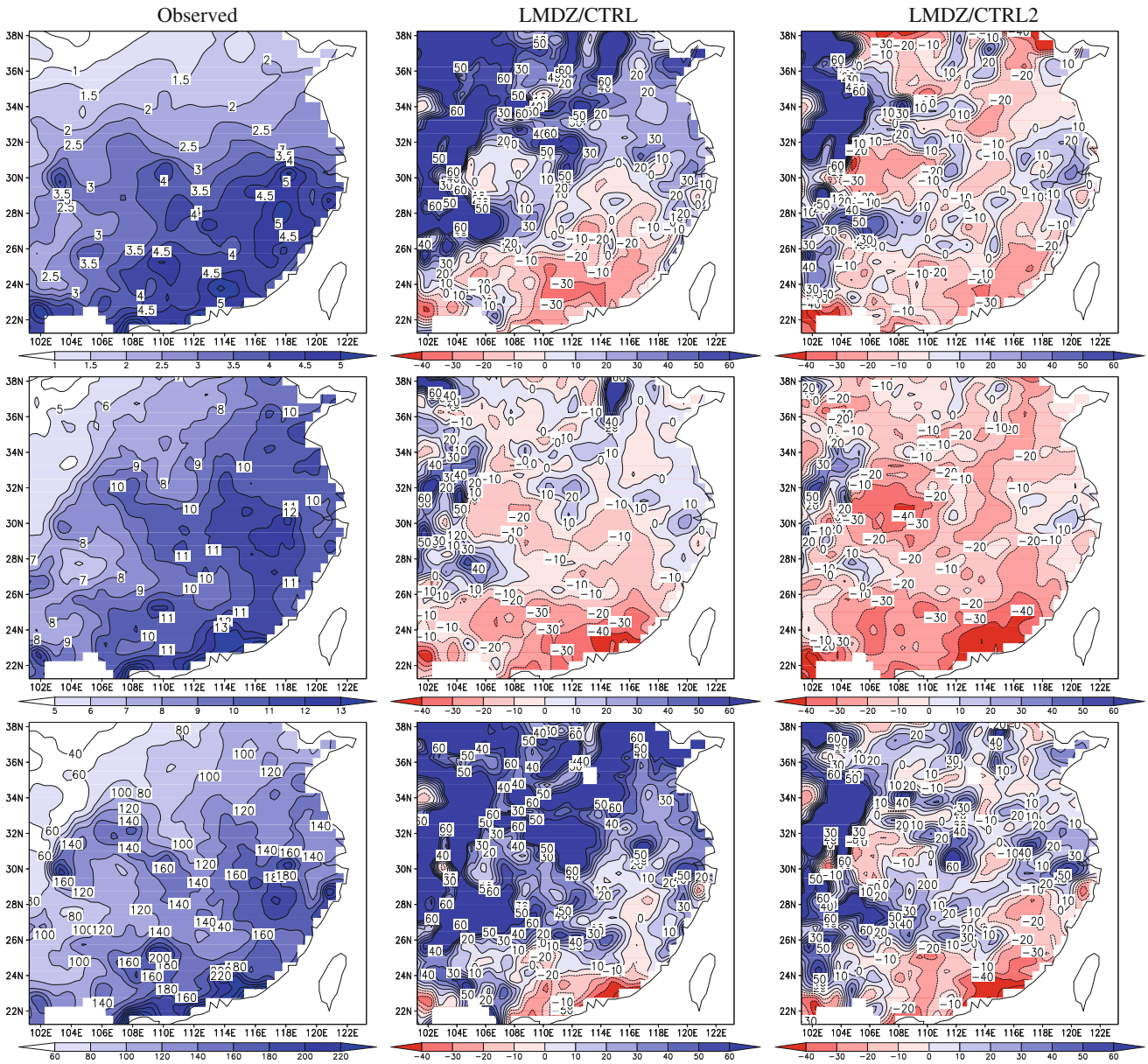

Fig. 4 Same as in Fig. 2, but for annual-mean precipitation rate (*top panels*, mm/day), SDII (*middle panels*, mm/day) and R5d (*bottom panels*, mm). Units of the fractional differences are %

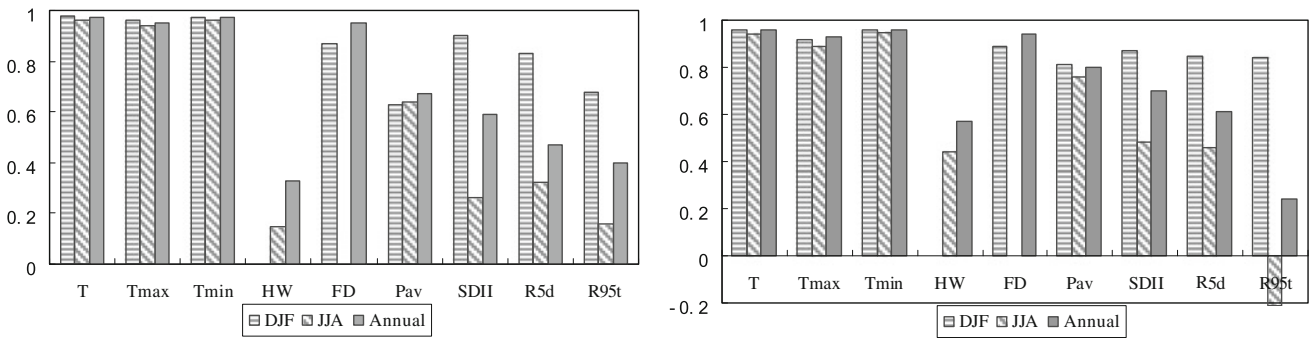

Fig. 5 Spatial-pattern correlation coefficients between the observed fields and simulated ones from LMDZ/CTRL (*left*) and LMDZ/CTRL2 (*right*)

Table 3 Domain-averaged biases of LMDZ in control simulations LMDZ/CTRL and LMDZ/CTRL2 (in parenthesis) in southeast China

	Temperature-based (model − observation)					Precipitation-based, % [(model − observation)/observed]			
	Tav	Tx	Tn	HW	FD	Pav	SDII	R5d	R95t
DJF	−3.5 (−1.5)	−3.3 (−1.3)	−4.5 (−2.6)	–	21.8 (12.3)	24.1 (43.8)	13.8 (10.7)	30.7 (44.9)	21.9 (19.6)
JJA	−0.7 (0.2)	−1.1 (0.01)	−0.7 (−0.04)	−0.1 (0.2)	–	17.1 (−2.9)	−11.9 (−30.8)	25.3 (−13.9)	31.1 (−2.3)
Annual	−1.8 (−0.4)	−1.9 (−0.3)	−2.3 (−1.1)	0.1 (1.2)	34.2 (19.8)	16.9 (−0.7)	−4.0 (−17.5)	35.5 (6.8)	27.2 (9.6)

Units are °C for Tav, Tx and Tn, days for HW and FD, % for all precipitation indices

3.2 Domain averages

In this section, we present a systematic evaluation of model performance by considering the domain averages. Table 3 summarizes the biases for winter, summer and annual mean for all indicators.

For temperature-based diagnostics, the most striking feature is the cold bias for both LMDZ/CTRL and LMDZ/CTRL2, larger in winter and smaller in summer. For instance, in winter the spatial averaged biases in LMDZ/CTRL for mean temperature, minimum temperature and maximum temperature are −3.5, −3.3, −4.5°C, respectively. The cold bias also implies biases in frost days (FD), which are much higher in simulations than in observations. For example, the annual number of frost days in LMDZ/CTRL is 34.2 days higher, compared to observation. Another indicator, HW, has a comparable magnitude in simulation and observation. Compared to the one-way nesting model, the most important improvement in the two-way nesting one is the reduction of the cold bias. For instance, in winter the spatial averaged biases in LMDZ/CTRL2 for mean temperature, minimum temperature and maximum temperature are −1.5, −1.3, −2.6°C, respectively, smaller than those of LMDZ/CTRL by about 2°C. We believe that the reduction of cold biases is due to the feedbacks from a detailed representation of climate in southeast China which can modify the large-scale atmospheric circulation (Fig. 3). Note that cold biases over this region have also been reported in a few other regional climate models (Fu et al. 2005; Tang et al. 2008).

We computed biases in the precipitation-based diagnostics as percentages of the observed values. We find different performance between LMDZ/CTRL and LMDZ/CTRL2. In general, there is a wet bias in LMDZ/CTRL: the domain averaged mean precipitation, R5d and R95t in LMDZ/CTRL is larger than observed for the two seasons (winter and summer) and annual. For example, in summer the relative biases between simulated and observed values for mean precipitation, R5d and R95t are +13.4, +23.7 and +32.7%, respectively. The SDII intensity indicator is lower than observations in summer and over the year. This is also because there are too frequent precipitation events (wet days) in LMDZ/CTRL (not shown) compared to observation. The two-way nesting model, LMDZ/CTRL2, has more precipitation in winter and less precipitation in summer, in comparison to the one-way nesting one. As a result, the former tends to overestimate the precipitation-based diagnostics in winter and underestimates the precipitation-based diagnostics in summer when compared with observed precipitation. For example in summer (JJA), the relative biases for mean precipitation (Pav), SDII, R5d and R95t in LMDZ/CTRL2 are −2.9, −30.8, −13.9 and −2.3%, respectively.

3.3 Added values of LMDZ-regional in simulating intense precipitation events

The joint utilization of LMDZ-global and LMDZ-regional allows us to assess the added values of the dynamical downscaling approach. Intuitively we can expect to improve the simulation of intense precipitation events through the dynamical downscaling. Our analysis focuses on daily precipitation characteristics in terms of the amount and frequency as a function of intensity. A precipitation event is defined as a daily precipitation value greater than or equal to 1 mm and dry days are removed. The data are then put into bins of 1 mm/day width starting at 1 mm/day. As in Gutowski et al. (2007) and Boberg et al. (2009), we normalize the frequency versus intensity distribution by dividing each bin frequency of events by the total number of precipitation events in all samples contributing to the distribution. We normalize the precipitation amount versus intensity distribution by dividing the amount for each bin by the total wet day precipitation amount for the 30-year reference period for southeast China. Results from surface gridded observations are also plotted as a reference.

Figure 6 shows the normalized frequency and amount of precipitation as a function of daily intensity for both observation and the reference simulations of LMDZ-Global, LMDZ/CTRL and LMDZ/CTRL2. In general the distribution of amount versus intensity is similar to that of frequency versus intensity. Extreme precipitation (e.g., greater than 50 mm/day) is more difficult to simulate in LMDZ-Global due to its coarse spatial resolution, characterized by a significant underestimation of the frequency and amount for intense events. However, both LMDZ/

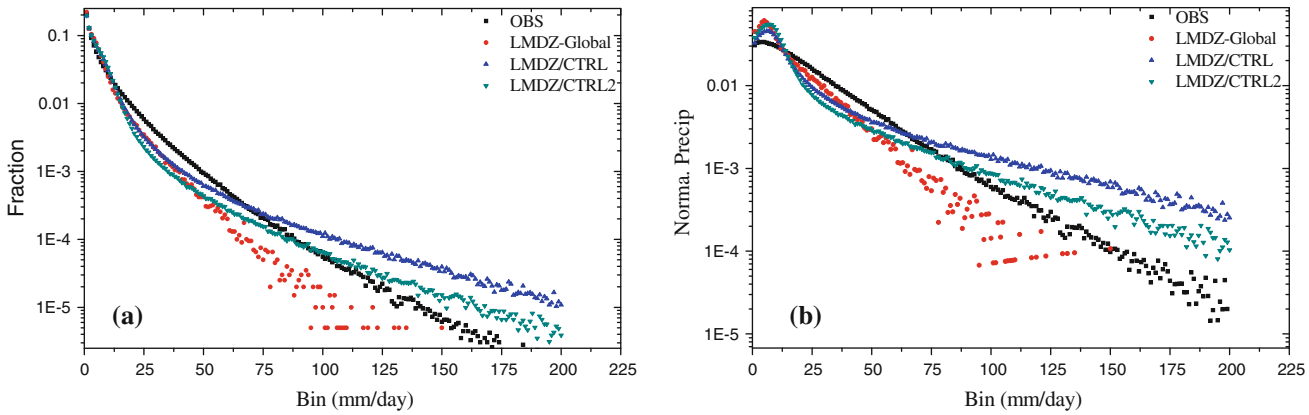

Fig. 6 **a** Normalized frequency and **b** amount of precipitation as a function of daily intensity for observation and the reference simulations of LMDZ-Global, LMDZ/CTRL and LMDZ/CTRL2

CTRL and LMDZ/CTRL2 show more extreme precipitation episodes (about 50 mm/day) than observations as well as LMDZ-Global, particularly for LMDZ/CTRL. We also find that precipitations in both LMDZ/CTRL and LMDZ/CTRL2 have a longer tails at high intensities, which are much closer to observations than LMDZ-Global, whose tail limit reaches only about 150 mm/day. In other words, only higher resolution models (LMDZ/CTRL and LMDZ/CTRL2) are capable of producing extreme precipitations (greater than 150 mm/day). The above results justify the use of finer scale models to simulate extreme events.

4 Projected changes of mean and extreme climate in southeast China

4.1 Temperature-based analyses

Figure 7 depicts the spatial distribution of the simulated change in annual-mean temperature for the four simulations (LMDZ/IPSL, LMDZ/IPSL2, LMDZ/CNRM and LMDZ/GFDL). We carried out a two-tailed *t* test to calculate the statistical significance of these changes. Areas where the change is statistically significant at the 95% confidence level are highlighted with stippling. The Tav changes are statistically significant at the 95% confidence level in all simulations and over the entire analysis area. All simulations show an increase in the whole region, with larger change (ranging from 1.6 to 2.2°C, depending on simulations) in the northern part of this region and smaller one in the south, where the magnitude is 1.2–1.6°C. Domain averaged changes in annual-mean temperature for the four simulations are 1.6, 1.5, 1.7 and 1.9°C, respectively. The spatial pattern of projected changes is generally similar in the four simulations. But a stronger zonal gradient can be observed in LMDZ/IPSL2 and the other three simulations have a more pronounced meridional gradient. This difference is also related to the difference of mean states in LMDZ/CTRL and LMDZ/CTRL2.

Figure 8 shows the change in the number of annual frost days. Significant decreases are projected to occur over whole southeast China among the four simulations, with values locally more intense in the western and central part of this region (the maximum value reaching 24 days), and smaller values in the southern part. The projected changes in number of annual frost days averaged over the region for the four simulations are 15, 15, 19 and 18 days, respectively. The main reason for the decrease of this index is due to the general rise in the daily minimum temperature (figures not shown).

In general, HW is projected to increase in China under A2 scenarios (Zhang et al. 2006). Figure 9 presents the pattern of changes in annual heat wave duration. For the four simulations, significant increases are projected over the entire region and reach a maximum of about 16 days in the southern part. Over the northern portions the increases are not as large as those in the southern, and reach only about 4–6 days.

A quantitative comparison is provided in Table 4, where the projected change in the domain-mean temperature diagnostics is listed for southeast China and for the four simulations (LMDZ/IPSL, LMDZ/IPSL2, LMDZ/CNRM and LMDZ/GFDL). Boldfaces represent the changes exceeding the 95% confidence level. It is clear that all the changes are statistically significant at the 95% confidence level. For all temperature-based diagnostics, the sign of change is consistent among the four simulations. Significant increases are projected in mean temperature, daily-maximum temperature and daily-minimum temperature, the signal has largest magnitude in winter, followed by the annual and summer. The number of frost days decreases significantly. For instance, the annual-mean frost days decrease by 12–18 days, depending on different simulations. On the

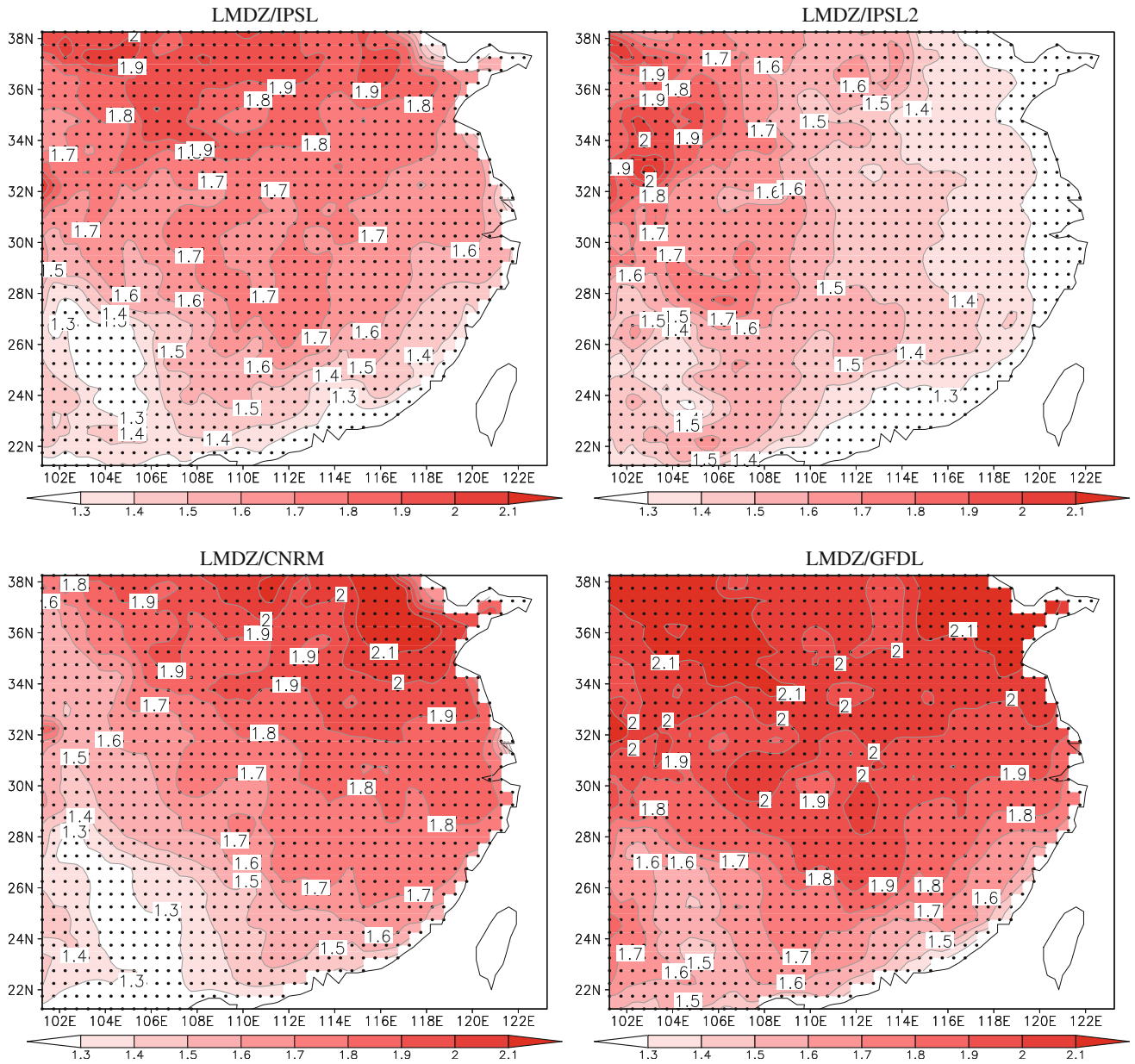

Fig. 7 Annual-mean temperature changes (future–present) from LMDZ/IPSL (*top left*), LMDZ/IPSL2 (*top right*), LMDZ/CNRM (*bottom left*), and LMDZ/GFDL (*bottom right*). Units are °C. Contour intervals are 0.1°C. *Stippling* indicates areas where the changes are statistically significant at the 95% confidence level

other hand, the heat wave days index over the whole region increases. For example, in summer, it increases by 6.2–7.2 days.

The general picture emerging from these analyses for temperature diagnostics is that the mean, maximum, minimum temperature increase over whole southeast China. As a result, the frost days decrease and the heat wave days increase significantly. There is a high coherence of changes among the four simulations (LMDZ/IPSL, LMDZ/IPSL2, LMDZ/CNRM and LMDZ/GFDL).

4.2 Precipitation-based analyses

Figure 10 shows the fractional change in annual-mean precipitation. Stippling indicates areas where the changes are statistically significant at the 95% confidence level. Clearly the stippling areas are much smaller than that of the temperature-based analyses. All simulations show an increase in the north of this region (north of 32°N) where the simulated change is 10-40%, and a transition to smaller changes or decreases in the southern part of this region.

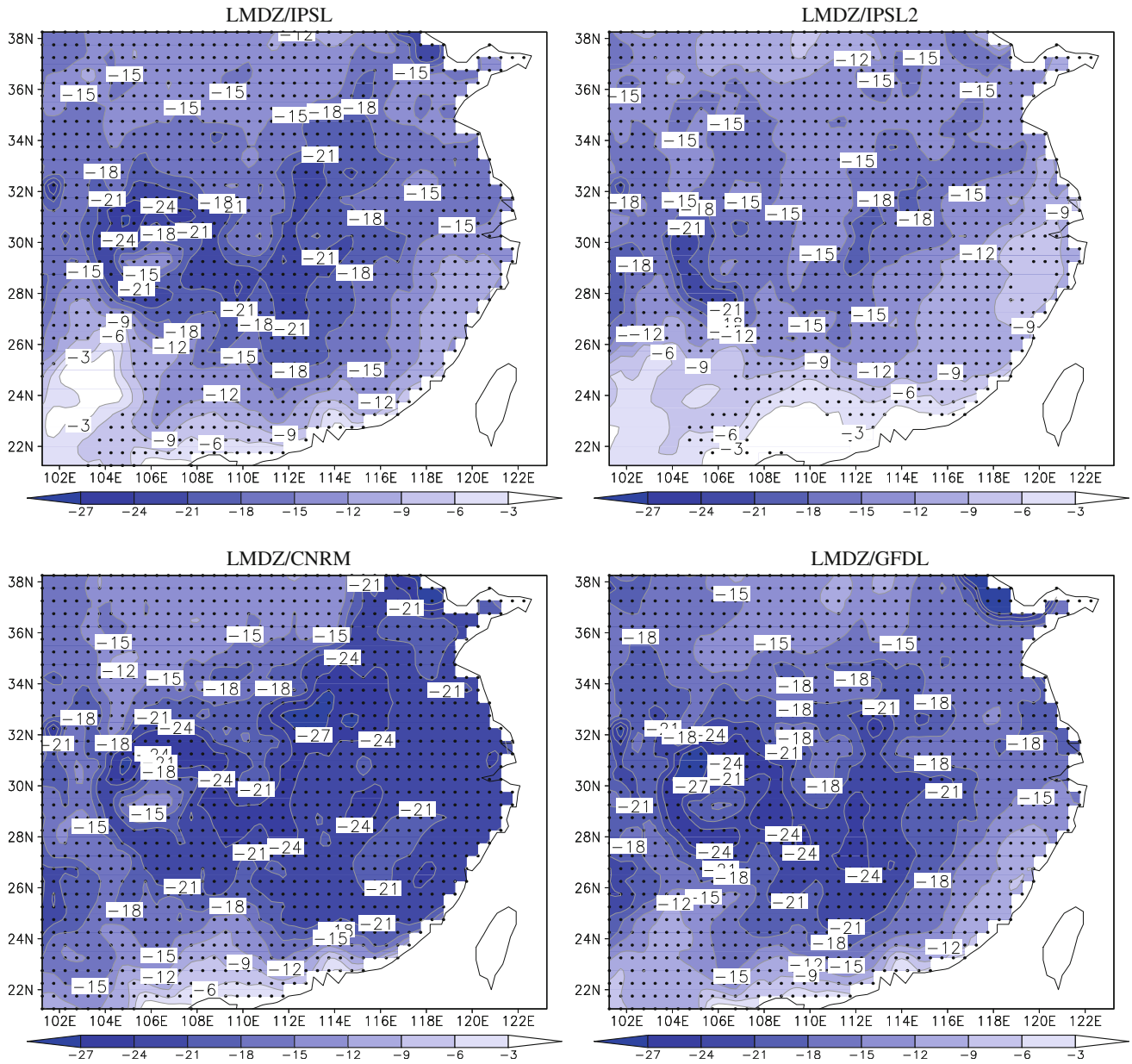

Fig. 8 Same as in Fig. 7, but for the annual number of frost days. Units are days and contour intervals are 3 days

The fractional change for R95t is provided in Fig. 11, which reveals a similar picture among the four simulations: R95t is projected to increase in some parts of this region in future, especially in the southern one where the projected annual total precipitation has no change or decreases, implying that the contributions to total precipitation from very high intensity events will increase under global warming, which is consistent with the explanation offered by Gutowski et al. (2007),where the change in intensity spectrum can be described by a gamma distribution that having a single transition point between precipitation rates that contribute more/less to the total precipitation.

A comparison of the precipitation diagnostics for winter (DJF), summer (JJA), and annual mean (Table 5) reveals larger dispersion in mean precipitation among the simulations than in mean temperature. For example, in winter, three simulations (LMDZ/IPSL, LMDZ/GFDL and LMDZ/IPSL2) show a decrease of 7–17%, but the other one, LMDZ/CNRM, shows an increase of 25%. It is interesting to note that the simulated changes in SDII, R5d, and R95t have the same sign for all seasons and for all simulations (an exception is for R5d in winter). For example the R95t is projected to increase by 11–14% in summer, suggesting that in general extreme precipitation

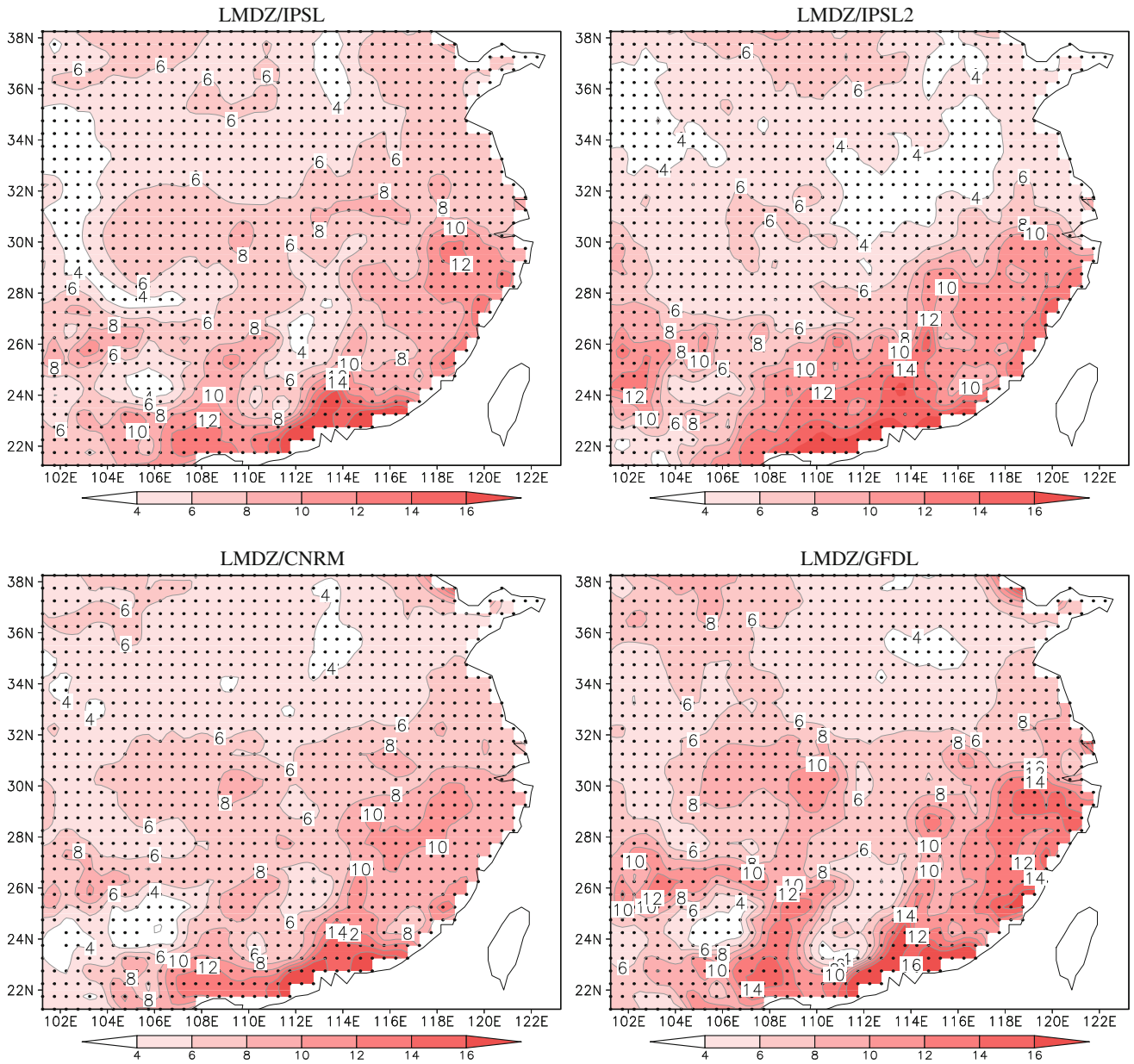

Fig. 9 Same as in Fig. 7, but for the annual heat wave duration. Units are days and contour intervals are 2 days

Table 4 Domain-averaged changes (future–present) for temperature diagnostics in southeast China

	DJF					JJA					Annual				
	Tav	Tx	Tn	HW	FD	Tav	Tx	Tn	HW	FD	Tav	Tx	Tn	HW	FD
LMDZ/IPSL	1.9	2.1	1.8	3.4	−6.8	1.5	1.6	1.5	6.3	−0.3	1.6	1.8	1.5	7.0	−15.0
LMDZ/CNRM	2.1	2.0	2.3	3.6	−9.9	1.6	1.5	1.7	5.9	−0.2	1.7	1.6	1.8	6.8	−18.8
LMDZ/GFDL	2.4	2.6	2.3	3.7	−9.2	1.8	1.9	1.9	7.6	−0.2	1.9	2.0	1.9	7.8	−17.5
LMDZ/IPSL2	1.8	2.0	1.7	3.3	−6.6	1.5	1.5	1.6	6.2	−0.2	1.5	1.6	1.5	7.0	−12.4

Units are °C for Tav, Tx and Tn, days for HW and FD. Boldfaces represent the changes exceeding the 95% confidence level

events will become more common in southeast China for the future under the IPCC A2 scenario. This conclusion is consistent with earlier studies (Zhang et al. 2006). The increase might be related to an intensification of the hydrological cycle associated with a warming-related increase of atmospheric moisture content (e.g., Frei et al.

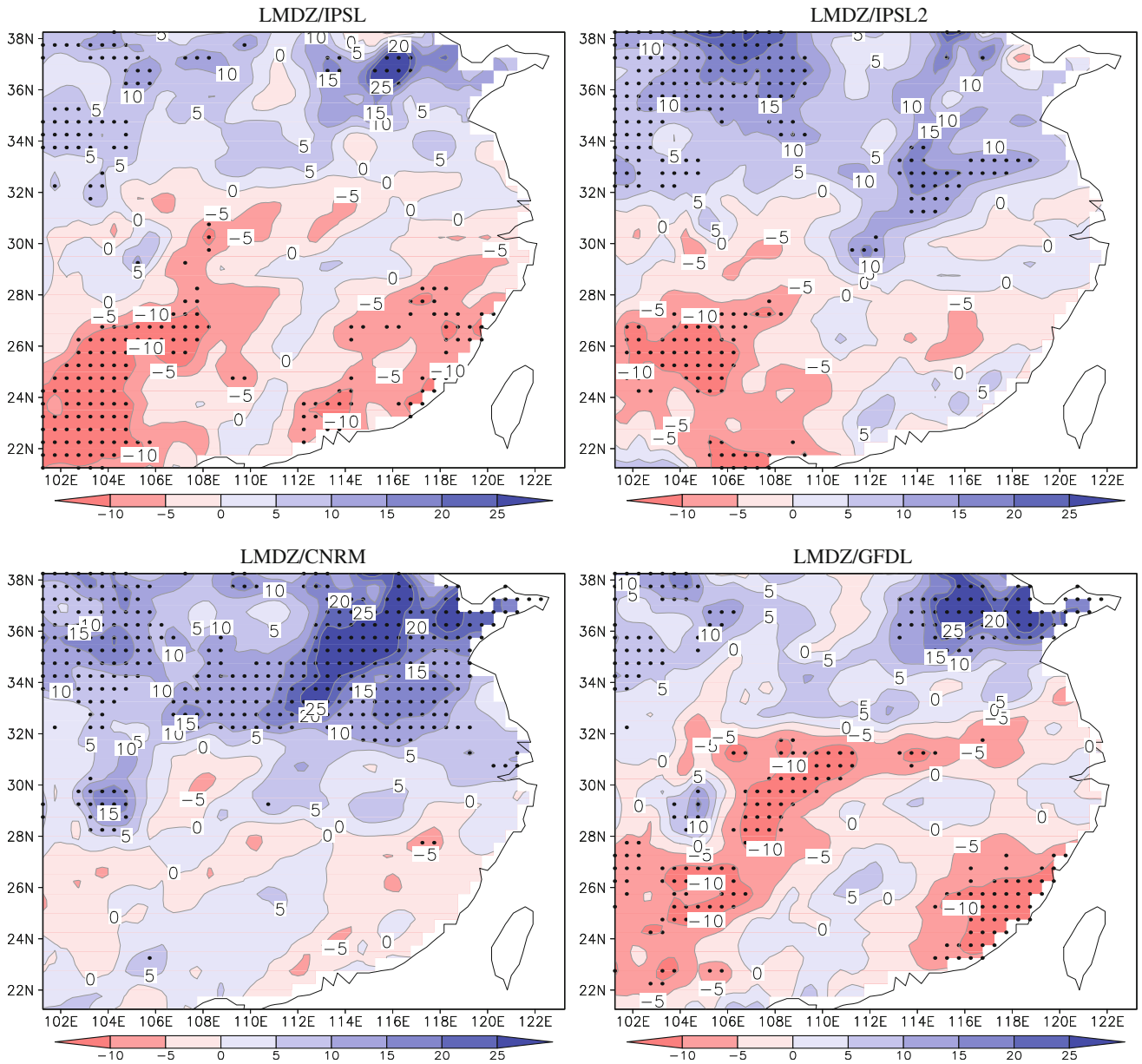

Fig. 10 Fractional change (future–present, in %) of annual-mean precipitation rate. *Stippling* areas indicate that the changes are statistically significant at the 95% confidence level. Contour intervals are 5%

1998; Allen and Ingram 2002; Trenberth et al. 2003; Meehl et al. 2005).

5 Conclusions

In the present study, we analyzed the potential changes of the mean climate as well as climate extremes in southeast China for the middle of the 21st century (about 2045), respective to a control period 1961/1990, under the SRES-A2 emission scenario. The simulations were performed with LMDZ-regional over southeast China. The lower boundary conditions (sea surface temperature and sea ice) were taken from three different global ocean–atmosphere coupled GCMs (IPSL, CNRM and GFDL) in order to estimate the robustness of the projection. Results from a two-way nesting system between LMDZ-global and LMDZ-regional were also presented. Besides the mean climate, we especially analyzed the projected change of extreme events, which were described in terms of extreme indices, such as the frost days, heat wave days, and heavy precipitation. The following conclusions can be drawn.

1. The evaluation of simulated temperature and precipitation for the current climate shows that in general

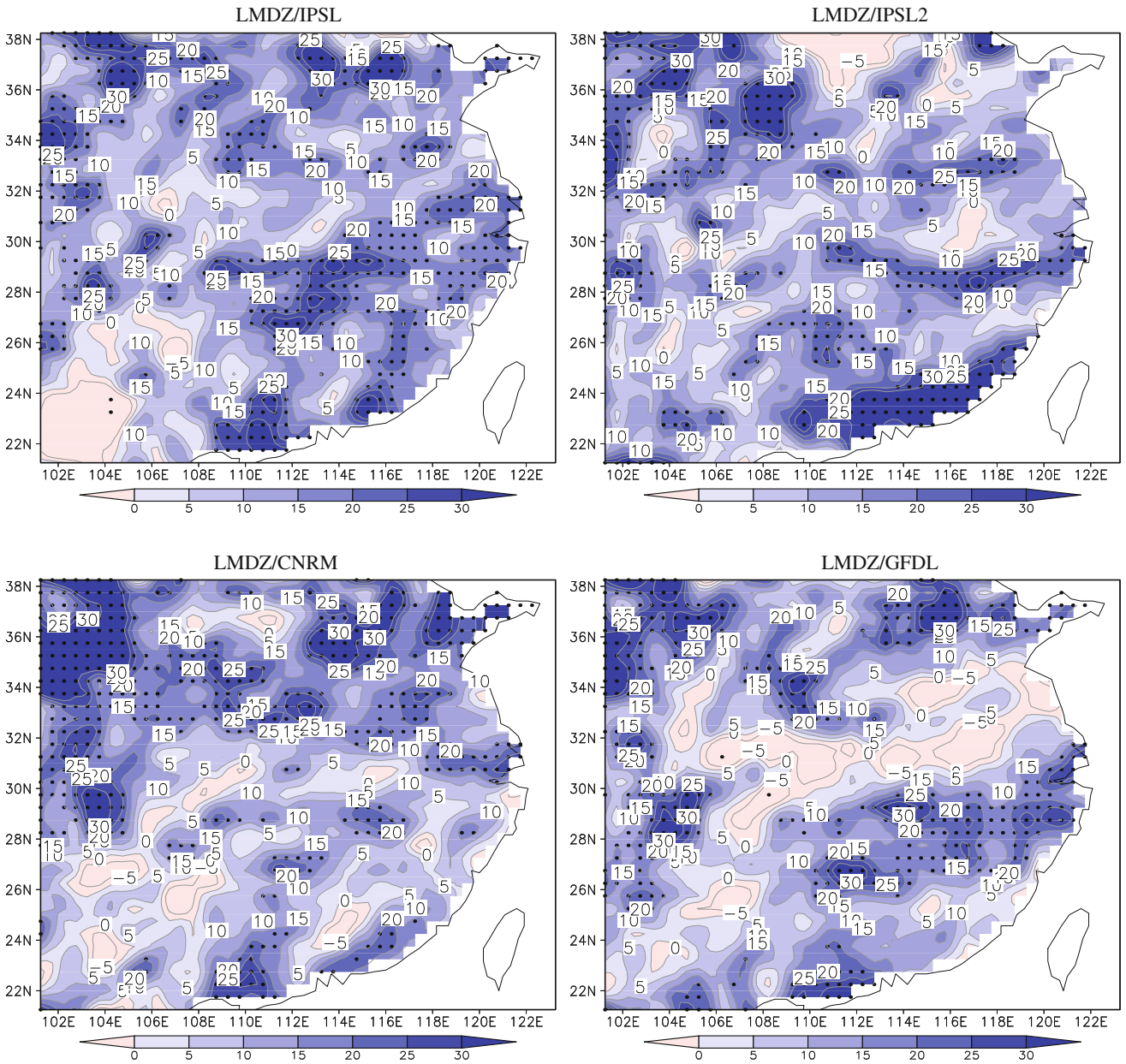

Fig. 11 Same as in Fig. 10, but for the annual-mean R95t. Contour intervals are 10%

Table 5 Fractional changes of domain-averaged precipitation diagnostics in southeast China

	DJF				JJA				Annual			
	Pav	SDII	R5d	R95t	Pav	SDII	R5d	R95t	Pav	SDII	R5d	R95t
LMDZ/IPSL	−7.0	7.3	5.7	**22.8**	1.4	**5.9**	**10.3**	**13.6**	−1.5	**7.0**	**10.3**	**13.6**
LMDZ/CNRM	**24.7**	**11.8**	**21.1**	**35.4**	**4.9**	**6.9**	**14.3**	**13.8**	**5.2**	**6.9**	**12.5**	**13.8**
LMDZ/GFDL	**−17.0**	2.9	−8.9	15.7	1.7	**4.2**	**11.0**	**11.3**	−0.9	**5.7**	**10.6**	**11.3**
LMDZ/IPSL2	**−12.2**	2.0	−4.4	8.9	3.4	**4.9**	**11.8**	**14.3**	1.0	**5.9**	**12.0**	**13.8**

Units are %. Boldfaces represent the changes exceeding the 95% confidence level

LMDZ-regional driven by LMDZ-global in one-way nesting reproduces well the spatial distribution of mean climate and extreme climate events in southeast China, and overall, the performance of LMDZ-regional for temperature-related indices is considerably better than for precipitation-related indices.

However, the model has a systematic cold bias in temperature and tends to overestimate the extreme precipitation. The two-way nesting model can reduce the "cold bias" to some extent compared to the one-way nesting model. This improvement is mainly due to feedbacks from LMDZ-regional to LMDZ-global which ameliorate the large-scale atmospheric circulation over southeast China.

2. Scenario results using IPCC SRES-A2 emissions show that in all seasons there is a significant increase for mean, daily-maximum and daily-minimum temperature in the entire region, associated with a decrease in the number of frost days and with an increase in the heat wave duration. The direction, magnitudes and main spatial patterns of the changes in temperature diagnostics show a quite good consistency among the three sets of lower-boundary conditions coming from three different global climate models. Two model configurations (LMDZ-global and LMDZ-regional working in tandem either sequentially or in a manner of two-way nesting) show also consistent results. Future projection of temperature-related indices is thus revealed to be of good confidence.
3. A warming environment gives rise to changes in extreme precipitation events. Precipitation extremes are generally projected to increase over most of southeast China, though mean precipitation may slightly decrease. This conclusion on precipitation extremes is less robust, since there exist considerable dispersions in magnitude of the projected changes in the four simulations. Besides, LMDZ/GFDL and LMDZ/IPSL2 even project a decrease in the maximum total precipitation during five consecutive days in winter.

As we use only one regional climate model driven by one global model under one emission scenario, we cannot fully explore uncertainties of future projection on climate extremes of both precipitation and temperature. It is clear that more research will be needed to assess the uncertainties on the projection in future of climate extremes. We need to include as many different types of downscaling models (e.g., dynamical and statistical downscaling), GCMs and emission scenarios as possible when generating climate-change information at the local scale. In this manner we can expect to construct a probabilistic projection for future evolution of climate extremes.

Acknowledgments Computer resources were allocated by the IDRIS, the computer centre of the CNRS. This work is supported by the Chinese NSF (National Science Foundation, No. 40875058), the National Key Technologies R&D Program under grant No. 2007BAC29B03, the natural science foundation of Jiangsu Province under grant No. 07KJA17020, the Research and Innovation Project for College Graduates of Jiangsu Province (No. CX09B_229Z), and the Sino-French cooperative project PRA 2007-15627TJ. IPSL SST and sea-ice concentration data are provided by Jean-Louis Dufresne and Laurent Fairhead. CNRM's SST and sea-ice data are provided by Michel Déqué. GFDL's SST and sea-ice data are downloaded from the web site: http://data1.gfdl.noaa.gov/nomads/forms/climate.html.

References

Alexander LV, Zhang X, Peterson TC, Caesar J, Gleason B, Klein Tank AMG, Haylock M, Collins D, Trewin B, Rahim F, Tagipour A, Kumar Kolli R, Revadekar JV, Griffiths G, Vincent L, Stephenson DB, Burn J, Aguilar E, Brunet M, Taylor M, New M, Zhai P, Rusticucci M, Luis Vazquez Aguirre J (2006) Global observed changes in daily climate extremes of temperature and precipitation. J Geophys Res 111:D05109. doi:10.1029/2005JD006290

Allen MR, Ingram WJ (2002) Constraints on future changes in climate and the hydrologic cycle. Nature 419:224–232

Boberg F, Berg P, Thejll P, Gutowski WJ, Christensen JH (2009) Improved confidence in climate change projections of precipitation evaluated using daily statistics from the PRUDENCE ensemble. Clim Dyn 32:1097–1106

Chen D, Ou T, Gong L, Xu CY, Li W, Ho CH, Qian W (2010) Spatial interpolation of daily precipitation in China: 1951–2005. Adv Atmos Sci. doi: 10.1007/s00376-010-9151-y (in press)

Delworth TL, Stouffer RJ, Dixon KW, Spelman MJ, Knutson TR, Broccoli AJ, Kushner PJ, Wetherald RT (2002) Review of simulations of climate variability and change with the GFDL R30 coupled climate model. Clim Dyn 19:555–574

Dufresne JL, Friedlingstein P, Berthelot M, Bopp L, Ciais P, Fairhead L, Le Treut H, Monfray P (2002) Effects of climate change due to CO_2 increase on land and ocean carbon uptake. Geophys Res Lett 29(10), 1405. doi:10.1029/2001GL013777

Frei C, Schär C, Lüthi D, Davies HC (1998) Heavy precipitation processes in a warmer climate. Geophys Res Lett 25(9): 1431–1434

Frei C, Schöll R, Fukutome S, Schmidli J, Vidale PL (2006) Future change of precipitation extremes in Europe: intercomparison of scenarios from regional climate models. J Geophys Res 111:D06105. doi:10.1029/2005JD005965

Frich P, Alexander LV, Della-Marta P, Gleason B, Haylock M, Klein Tank AMG, Peterson T (2002) Observed coherent changes in climatic extremes during the second half of the 20th century. Clim Res 19:193–212

Fu C, Wang S, Xiong Z et al (2005) Regional climate model intercomparison Project for Asia. Bull Am Meteorol Soc 86:257–266

Gao XJ, Lin WT, Fred K, Zhao ZC (2004) Simulation of climate and short-term climate prediction in China by CCM3 driven by observed SST. Chin J Atmos Sci 28:78–90 (in Chinese with English abstract)

Gao X, Xu Y, Zhao ZC, Pal JS, Giorgi F (2006) On the role of resolution and topography in the simulation of East Asia precipitation. Theor Appl Climatol 86:173–185

Gao X, Shi Y, Song R, Giorgi F, Wang Y, Zhang D (2008) Reduction of future monsoon precipitation over China: comparison between a high resolution RCM simulation and the driving GCM. Meteorol Atmos Phys 100:73–86

Gastineau G, Li L, Le Treut H (2009) The Hadley and Walker circulations changes in global warming conditions described by idealized atmospheric simulations. J Clim 22:3993–4013

Gibelin AL, Déqué M (2003) Anthropogenic climate change over the Mediterranean region simulated by a global variable resolution model. Clim Dyn 20:327–339

Goodess CM (2003) Statistical and regional dynamical downscaling of extremes for European regions: STARDEX, Eggs 6:25–29. http://www.the-eggs.org/

Goodess CM, Hall J, Best M, Betts R, Cabantous L, Jones PD, Kilsby CG, Pearman A, Wallace CJ (2007) Climate scenarios and decision making under uncertainty. Built Environ 33(1):10–30

Goubanova K, Li L (2007) Extremes in temperature and precipitation around the Mediterranean basin in an ensemble of future climate scenario simulations. Glob Planet Change 57:27–42

Gutowski WJ Jr, Kozak KA, Arritt RW, Christensen JH, Patton JC, Takle ES (2007) A possible constraint on regional precipitation intensity changes under global warming. J Hydrometeorol 8:1382–1396

Haylock MR, Cawley GC, Harpham C, Wilby RL, Goodess CM (2006) Downscaling heavy precipitation over the United Kingdom: a comparison of dynamical and statistical methods and their future scenarios. Int J Climatol 26:1397–1415

Hourdin F, Musat I, Bony S, Braconnot P, Codron F, Dufresne JL, Fairhead L, Filiberti MA, Friedlingstein P, Grandpeix JY, Krinner G, LeVan P, Li ZX, Lott F (2006) The LMDZ4 general circulation model: climate performance and sensitivity to parametrized physics with emphasis on tropical convection. Clim Dyn 27:787–813. doi:10.1007/s00382-006-0158-0

Hundecha Y, Bardossy A (2008) Statistical downscaling of extremes of daily precipitation and temperature and construction of their future scenarios. Int J Climatol 28:589–610

Jiang D, Wang HJ, Lang X (2005) Evaluation of east Asian climatology as simulated by seven coupled models. Adv Atmos Sci 22:479–495

Jiang ZH, Chen WL, Song J, Wang J (2009) Projection and evaluation of the precipitation extremes indices over China based on seven IPCC AR4 coupled climate models. Chin J Atmos Sci 33:109–120 (in Chinese with English abstract)

Jones RG, Noguer M, Hassell D, Hudson D, Wilson S, Jenkins G, Mitchell J (2004) Generating high resolution climate change scenarios using PRECIS, report, Met Off. Hadley Centre, Exeter

Li ZX (1999) Ensemble atmospheric GCM simulation of climate interannual variability from 1979 to 1994. J Clim 12:986–1001

Liu Y, Bao Q, Duan A, Qian Z, Wu G (2007) Recent progress in the impact of the Tibetan Plateau on climate in China. Adv Atmos Sci 24:1060–1076

Lorenz P, Jacob D (2005) Influence of regional scale information on the global circulation: a two-way nesting climate simulation. Geophys Res Lett 32:L18706. doi:10.1029/2005GL023351

Meehl GA, Arblaster JM, Tebaldi C (2005) Understanding future patterns of increased precipitation intensity in climate model simulations. Geophys Res Lett 32:L18719. doi:10.1029/2005GLO23680

Meehl GA, Stocker TF, Collins WD, Friedlingstein P et al (2007) Global climate projections. In: Solomon S, Qin D, Manning M, Chen Z, Marquis M, Averyt KB, Tignor M, Miller HL (eds) Climate change 2007: the physical science basis. Contribution of Working Group I to the 4th assessment Report of the IPCC. Cambridge University Press, Cambridge, pp 747–846

Schmidli J, Goodess CM, Frei C, Haylock MR, Hundecha Y, Ribalaygua J, Schmith T (2007) Statistical and dynamical downscaling of precipitation: an evaluation and comparison of scenarios for the European Alps. J Geophys Res 112:D04105. doi:10.1029/2005JD007026

STARDEX (2005) STARDEX: downscaling climate extremes. Climatic Research Unit, School of Environmental Sciences, University of East Anglia, 24 pp

Tang JP, Chen X, Zhao M, Su BK (2008) Numerical simulation of regional climate change under IPCC A2 scenario in China. Acta Meteorologica Sinica 66:13–25 (in Chinese with English abstract)

Tebaldi C, Hayhoe K, Arblaster JM, Meehl GA (2006) Going to the extremes: an intercomparison of model-simulated historical and future changes in extreme events. Clim Change 79:185–211

Trenberth KE, Dai A, Rasmussen RM, Parsons DB (2003) The changing character of precipitation. Bull Am Meteorol Soc 84:1205–1217

Uppala SM, et al (2005) The ERA-40Re-Analysis. Q J Roy Meteor Soc 131:2961–3012. doi:10.1256/qj.04.176

Wang J, Jiang ZH, Song J, Ding YG (2008) Evaluating the Simulation of the GCMS on the Extreme Temperature Indices in China. Acta Geographica Sinica 63:228–236 (in Chinese with English abstract)

Wetterhall F, Bárdossy A, Chen D, Halldin S, Xu CY (2006) Daily precipitation downscaling techniques in different climate regions in China. Water Resour Res 42:W11423. doi:10.1029/2005WR004573

Wilby RL, Charles SP, Zorita E, Timbal B, Whetton P, Mearns LO (2004) Guidelines for use of climate scenarios developed from statistical downscaling method, technical report. Data Distribution Centre of the Intergovernmental Panel on Climate, Norwich

Wu G, Liu Y, Wang T, Wan R, Liu X, Li W, Wang Z, Zhang Q, Duan A, Liang X (2007) The influence of mechanical and thermal forcing by the Tibetan Plateau on Asian climate. J Hydrometeorol 8:770–789

Xie P, Chen M, Yang S, Yatagai A, Hayasaka T, Fukushima Y, Liu C (2007) A gauge-based analysis of daily precipitation over east Asia. J Hydrometeorol 8:607–626

Xu Y, Gao X, Shen Y (2009) A daily temperature dataset over China and its application in validating a RCM simulation. Adv Atmos Sci 26(4):763–772

Zhang Y, Xu YL, Dong WJ (2006) A future climate scenario of regional changes in extreme climate events over China using the PRECIS climate model. Geophys Res Lett 33:L24702. doi:10.1029/2006GL027229

Zhou TJ, Li ZX (2002) Simulation of the East Asian summer monsoon by using a variable resolution atmospheric GCM. Clim Dyn 19:167–180

Zhou TJ, Yu RC (2006) 20th century surface air temperature over China and the globe simulated by coupled climate models. J Clim 19:5843–5858

Zou LW, Zhou TJ, Li L, Zhang J (2010) East China Summer Rainfall Variability of 1958–2000: dynamical downscaling with a variable-resolution AGCM. J Clim (in press)